DARU Journal of Pharmaceutical Sciences (2019) 27:9–20
https://doi.org/10.1007/s40199-018-0232-2

RESEARCH ARTICLE

Adsorption and in vitro release study of curcumin form polyethyleneglycol functionalized multi walled carbon nanotube: kinetic and isotherm study

Somayeh Koupaei Malek[1] · Mohammad Ali Gabris[1] · Binta Hadi Jume[1] · Raheleh Baradaran[1] · Madzlan Aziz[1] · Khairil Juhanni Bt. Abd Karim[1] · Hamid Rashidi Nodeh[2]

Received: 28 September 2018 / Accepted: 3 December 2018 / Published online: 15 December 2018
© Springer Nature Switzerland AG 2018

Abstract

Polyethylene glycol functionalized with oxygenated multi-walled carbon nanotubes (O-PEG-MWCNTs) as an efficient nanomaterial for the in vitro adsorption/release of curcumin (CUR) anticancer agent. The synthesized material was morphologically characterized using scanning electron microscopy, Fourier transform infrared spectroscopy and transmission electron microscopy. In addition, the CUR adsorption process was assessed with kinetic and isotherm models fitting well with pseudo-second order and Langmuir isotherms. The results showed that the proposed O-PEG-MWCNTs has a high adsorption capacity for CUR (2.0×10^3 mg/g) based on the Langmuir model. The in vitro release of CUR from O-PEG-MWCNTs was studied in simulating human body fluids with different pHs (ABS pH 5, intestinal fluid pH 6.6 and body fluid pH 7.4). Lastly, to confirm the success compliance of the O-PEG-MWCNT nanocomposite as a drug delivery system, the parameters affecting the CUR release such as temperature and PEG content were investigated. As a result, the proposed nanocomposite could be used as an efficient carrier for CUR delivery with an enhanced prolonged release property.

Keywords Multi walled carbon nanotubes · Curcumin · Adsorption isotherm · Release · Drug delivery

Introduction

Curcumin (CUR) is a natural compound known as a potent nontoxic, antioxidant, anti-tumor and anti-inflammatory agent with a variety of therapeutic properties such as anti-HIV, anti-bacterial, anti-oxidant, anti-carcinogenic, anticoagulation, antifungal, and antiseptic activities, most interestingly with nontoxic side effects even at high dosages [1–3]. Nevertheless, CUR suffers from the low water solubility and low bio-stability in the human body during the metabolism process, and also it could be affected by some enzyme activities [4, 5]. Therefore, to enhance its solubility and biocompatibility, it is essential to provide the drug with a suitable delivery system [6, 7].

Recently, carbon based nano material has gained a considerable attention leading to a great breakthrough in nanotechnology for its unique physical properties, surface chemistry and structure [8, 9]. Particularly, carbon nanotubes (CNTs) holds tremendous potentials in many fields especially biological and biomedical domains as an ideal material for several applications [10, 11]. CNTs are known as superior adsorbents for their unique one-dimensional tubular structure, the tendency to establish strong electrostatic π-π interactions and high surface area [12]. CNT could be used as a molecular delivery system for transporting biological molecules including DNA and RNA [13]. Interestingly, to enhance its reactivity and also to provide more active accommodating sites (in order to increase the delivering capacity), CNT's surface could be easily functionalized and various groups could be introduced to it for medical purposes [14, 15]. CNT seems to be very dynamic and applicable in biological applications due to its special one-dimensional nano-hollow-tubular structure and high surface area [16] as well as CNTs

✉ Madzlan Aziz

✉ Hamid Rashidi Nodeh
rnhamid2@gmail.com

[1] Universiti Teknologi Malaysia, Johor Bahru, Johor, Malaysia

[2] Department of Food Science & Technology, Faculty of Food Industry and Agriculture, Standard Research Institute (SRI), Karaj P.O. Box: 31745-139, Iran

developed as emerging cancer cell delivery system [15]. Moreover, non-covalent π-π interactions allow an easy and high drug loading capacity on the outside, inside and the sidewall providing a prolonged blood circulation and high stability with minimum toxicity side effects in the body [17–20]. However, very few have reported the adsorption/release of CUR drugs onto such a high potential material (CNT loaded systems) [21, 22] [23]. To date, some studies have stated the successful adsorption and desorption of various drugs such as curcumin, doxorubicin and mitoxantrone onto CNTs [23, 24]. However, there are two main problems with using CNTs, the lack of biocompatibility and poor solubility, and the very high surface area holding toxic effects inside the human body [25]. The oxidation of CNT as a hydrophobic material is a very common modification method generating hydrophilic oxygen-containing functional groups which enhances the adsorption capacity and solubility, and facilitates additional functionalization of CNT [19, 26]. A suitable functionalization of CNT is recommended to produce a less toxic biocompatible system with an increased solubility and to protect the carried drug [27]. One of the best approaches is the covalent anchorage of polyethylene glycol (PEG) segments on the CNT walls offering some therapeutic advantages including low toxicity, good aqueous dispensability and most importantly a prolonged circulation time and a more efficient drug release system which is induced by the dense brushes of PEG [28, 29]. In addition, it is noteworthy that PEG-modified CNTs shows an improved bioavailability and biocompatibility, increased uptake and therapeutic efficacy. The high molecular weight and hydrophilic nature of PEG offers a higher physical and chemical stability to the final solid matrix and makes the drug less prone to denaturation [30]. It increases both the drug-carrier interactions and the loading capacity [13, 18, 31]. PEG is a dual nature material soluble in both water and organic solvents, besides PEGylation can increase the bioavailability of the delivery systems [32]. This, by adding a hydrophilic character to CNT, could improve its accessibility and dispersibility in the aqueous circulating blood or body fluids [33].

To the best of our knowledge, no studies have been conducted on the adsorption and desorption of curcumin onto PEG polymer-oxygenated MWCNTs nanocomposite (O-PEG-MWCNTs) with the aim of developing a more efficient drug delivery system. In this study, the adsorption and desorption of CUR on a novel synthesized O-PEG-MWCNTs was investigated. Adsorption kinetics, adsorbent isotherm and CUR desorption in simulated solution were all studied. CUR adsorption mechanism onto O-PEG-MWCNTs could be explained via π-π interaction, hydrophobic and hydrogen bonding.

Material and methods

Materials

All chemicals were of the high analytical grade. Multi-wall carbon nanotube MWCNT (purity 95%, 0.5-2 m in length) was purchased from Chengdu Organic Chemicals Co.Ltd. Curcumin was bought from Carlroth gambH.co. DMAP 99% (dimethyl amino pyridine), EDC (1-ethyl-3 (3 dimethylaminopropyl) and carbodiimide were supplied from Merck. PEG (MW = 6000 Da) was purchased from Sigma. H_2SO_4 (95%) and HNO_3 (65%) were supplied from QRec. HPLC grade Acetonitrile and Methanol were bought from J.T.Baker.

Instrumentation

The FTIR spectra were recorded using a Perkin Elmer FT-IR spectrometer (MA, USA) operating in the range of 450 to 4000 cm^{-1}. The surface morphology analysis of the nanocomposite was performed using a JEOL-JSM-6701F (Tokyo, Japan) field emission scanning microscopy equipped with an energy dispersive X-ray spectroscopy. Thermogravimetric analysis (TGA) was studied with Pyris Diamond from PerkinElmer (Yokohama, Japan) at temperature of 30 to 800 °C with rate of 20 °C/min. The high detailed nanostructure of O-PEG-MWCNTs was examined using a JEOL-JEM-2100 (Tokyo, Japan) transmission electron microscope. An Agilent 1100 series liquid chromatography (HPLC-UV) with a C-18 column (particle size 5 μm, 4.6 mm and 20 mm) was used for CUR analysis at a wavelength of 425 nm. An isocratic mobile phase (acetonitrile/water 70:30) was used for CUR analysis with a constant fellow rate of 1 mL/min.

Oxidation of MWCNTs

MWCNTs were treated and activated with a solution composed of 65% H_2SO_4/95% HNO_3 in a volume ratio of 3:1 as a liquid phase oxidant referring to our previous work [34]. Typically, raw CNTs were refluxed under stirring in nitric acid (HNO_3 30% concentration) at 130 °C for three hours. Then, the mixture was filtered after being cooled down to the room temperature and washed with deionized water to obtain purified oxidized MWCNTs. The suspension was sonicated for one hour at a temperature lower than 50 °C to avoid the structural damage. After that distilled water was added to the suspension, then separation was carried out by centrifugation. Lastly, the resulting solid (O-MWCNTs) was filtered and carefully washed with deionized water until being neutralized (pH~7), and the sample was dried in a vacuum oven at 80 °C.

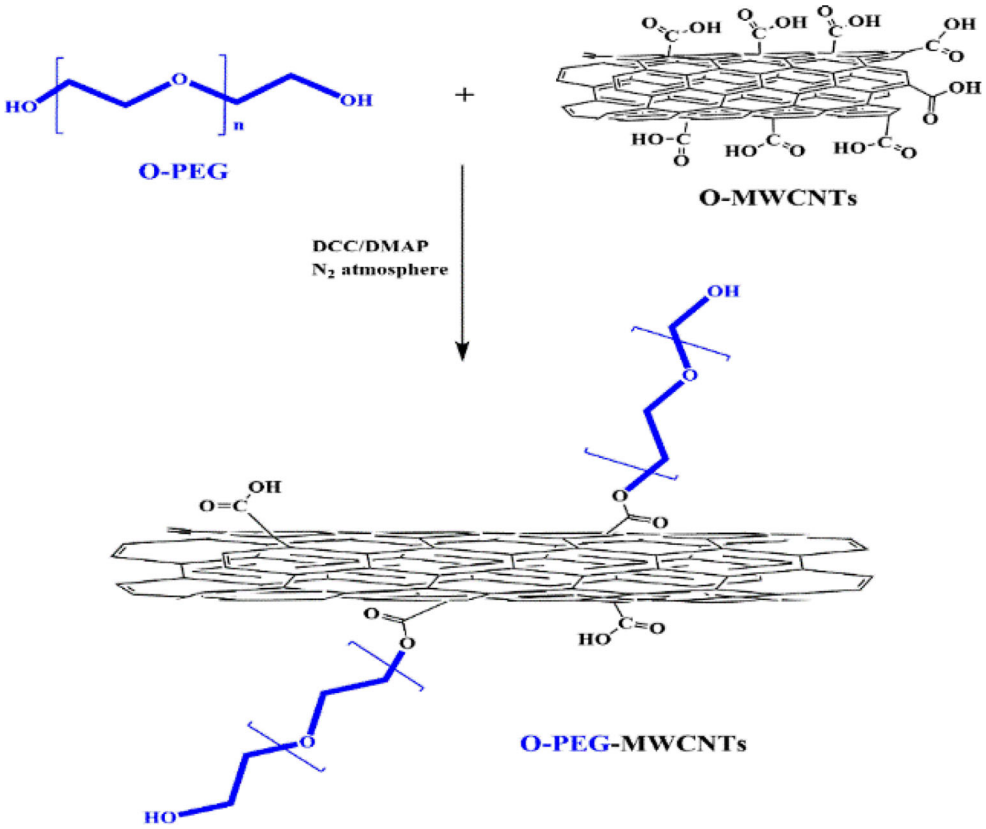

Fig. 1 Synthesis route for preparation O-PEG-MWCNT nanocomposite

Preparation of O-PEG-MWNTs

The functionalization of O-MWNTs with PEG was initiated via a carbodiimide-activated esterification reaction as illustrated in Fig. 1. Herein EDC (2.5 mmol) and DMAP (0.084 mmol) were mixed and added into the suspension of O-MWCNTs (500 mg) and PEG-6000 (50 mg) in 250 mL dichloromethane (CH_2Cl_2) solvent. The mixture was then stirred at the room temperature under the nitrogen atmosphere (gas flow) for 24 h. Thereafter, the mixture was diluted by CH_2Cl_2, vacuum filtered through a PTFE (0.2 μM) membrane and washed with CH_2Cl_2 and excess deionized water. Lastly, the black solid powder product was collected and dried in an oven at 40 °C for 5 h.

Batch adsorption of CUR onto O-PEG-MWCNTs

First, different concentrations of CUR (50–1000 mg/L) were prepared in batch and mixed with 10 mg of O-PEG-MWCNT in conical flasks under the ultra-sonication (wrapped with aluminium foil) for 5–48 h followed by shaking at 250 rpm at the room temperature. Afterwards, they were centrifuged at 5000 rpm for 20 min and the suspension was filtered via membranes with pore sizes of 0.2 μm diameter (in order to get clear solution for HPLC analysis). Then, the residual concentration of the CUR drug was analyzed using an HPLC-UV at the wavelength of 425 nm. The residual and released concentration of adsorbate (CUR) was obtained from the external calibration curve using standard CUR solutions. Thereafter, the experimental adsorption data was collected and adsorption efficiency ($R\%$) and adsorption capacity (q_e, mg/g) were calculated using Eqs. (1) and (2) as follow;

$$q_e = [V \times (C_0 - C_e)]/m \quad (1)$$

$$\%R = [(C_0 - C_e)/C_0] \times 100 \quad (2)$$

Wherein, C_e and C_o are the concentrations of CUR after and before adsorption in mg/L, V is the sample volume in liters (L) and m is the adsorbent mass in grams (g).

Release or desorption of CUR from O-PEG-MWCNT

CUR desorption or release from the O-PEG-CNT-CUR suspension was performed in a simulated intestinal fluid (SIF, pH 6.6) and a simulated body fluid (SBF, pH 7.4) at the normal human body temperature of 37 °C under a 100 rpm stir on an orbital shaker (Max QTM 4000 series; Thermo Fisher). Briefly, 5 mg of PEG-CNT-CUR was transferred into 5 mL SIF or SBF solution in a 10 mL tube. At predetermined times (0.5–96 h) the tube was centrifuged for 20 min (5000 rpm) and the supernatant was stored in a sealed sample bottle at 4 °C in dark.

The collected supernatants were analyzed for absorbance at λ = 425 nm with HPLC-UV. The desorption or release percentage was calculated according to Eq. (3) [35, 36]:

$$Desorption\% = \frac{C_R}{C_L} \times 100 \quad (3)$$

Where C_R is the released CUR concentration in the eluent (mg/L) and C_L is the loaded amount of CUR onto O-PEG-MWCNTs (mg/L).

Results and discussion

Characterization

FTIR spectroscopy: surface functional groups of the neat PEG, oxygenated MWCNTs and polymerized nanocomposites (O-PEG-MWCNT) were examined using FTIR spectroscopy. The results are summarized in Fig. 2a, b & c. All materials exhibited a broad absorption band in the range of 3400–3550 cm^{-1} which could be assigned to the stretching vibrations of hydroxyl groups (OH). The absorption peaks around 1620, 1643, 1634 corresponding to O-H from water. The sharp band at 1399 cm^{-1} (Fig. 2b) clearly imply the presence of conjugated C=C (sp^2) bonding of the aromatic carbon structure array of the MWCNT material which are excluded in the neat PEG spectrum. The absorption band at 1732 cm^{-1} and 1712 cm^{-1} wre due to the carbonyl (C=O) group of the activated MWCNT. As shown in Fig. 2 (a) and (c) the bands corresponding to C–H stretching from PEG and O-PEG-MWCNT are observed at 2909 and 2210 cm^{-1}. The peaks noted at 1298, 1217, 1099 and 1011 cm^{-1} are related to stretching C–O–C and C-O-H (vibrations in the PEG chain and also the presence of PEG in the final O-PEG-MWCNT nanocomposite product [33]. Hence, most notable is the appearance and disappearance of some new band verifying the interfacial covalent bonding between O-MWCNTs and PEG and the successful assembly of the two components.

FESEM/EDX analysis: Fig. 3(a) and (b) showed the morphology of MWCNT respectively before and after polymerization. There are two clear aspects to be observed, the severe agglomeration and the entanglement of pristine CNTs forming cotton-like agglomerates [37, 38]. However, the synthesized O-PEG-MWCNTs shows clearer single long CNT threads, a better dispersion and larger surface area with less entangled CNTs and agglomerates. It also maintains the whole structure with no collapse after the oxidation [26]. EDX spectrum (Fig. 3c) proved the presence of the expected elements for pristine MWCNTs as carbon (81%), oxygen (9%) and some impurities of metal catalysts (i.e., Ni, Al, Si ~10%). The O-PEG-MWCNTs provided 80% carbon and 18% oxygen and only 2% impurities. This shows an increase in the amount of oxygen in O-PEG-MWCNTs compared to the oxygenated CNTs. The decrease in impurities may be associated with the oxygenation step in which by using acids the metal catalysts were removed [38, 39].

TEM analysis: The TEM micrograph of the O-PEG-MWCNTs with 10 nm magnification is illustrated in Fig. 3(d). Corresponding to the structure of MWCNTs and revealed the multi graphitic layered pattern represented by the lines embracing the hollow inner core of the MWCNTs tubes. The successful PEGylating of CNTs was confirmed through the rough thicker surface and wrinkles appearing darker

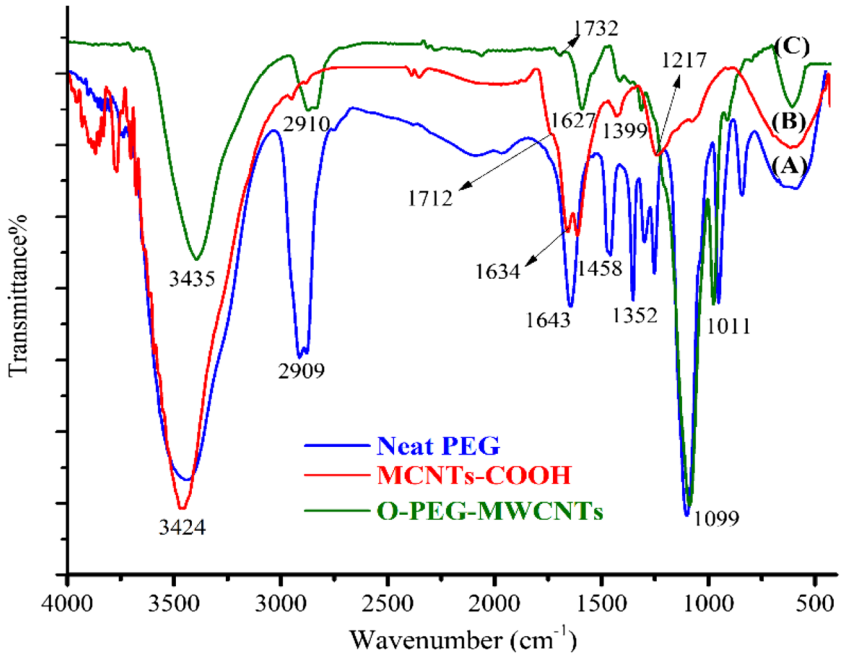

Fig. 2 The FTIR spectra for oxygenated MWCNT, neat PEG and O-PEG-MWCNT

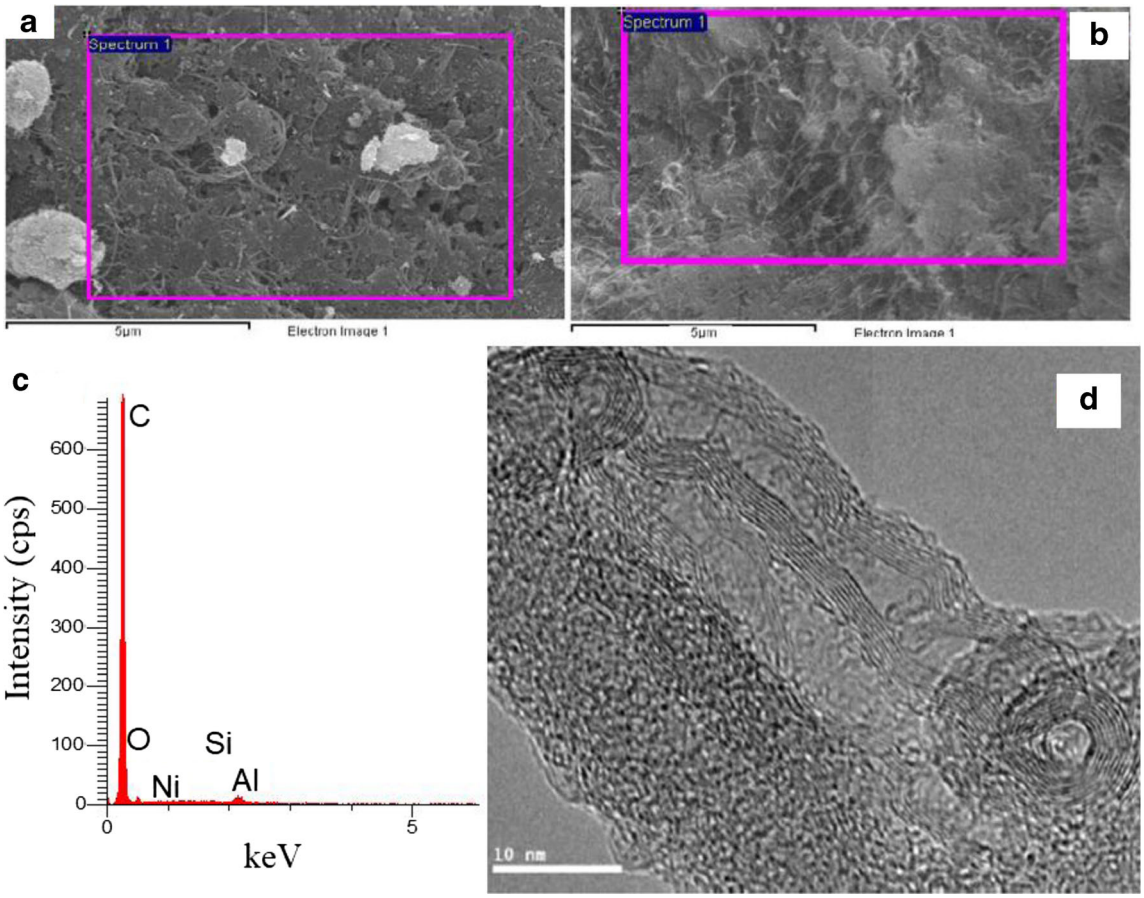

Fig. 3 FESEM/EDX images of (**a**) MWCNT and (**b**) O-PEG-MWCNT, (**c**) EDX spectra and (**d**) is TEM image of O-PEG-MWCNT adsorbed CUR

coverage [40]. Lastly, the TEM micrographs showed curvy MWCNTs in various size distribution with some aggregation that probably is due to the intermolecular forces sticking the tubes together [38].

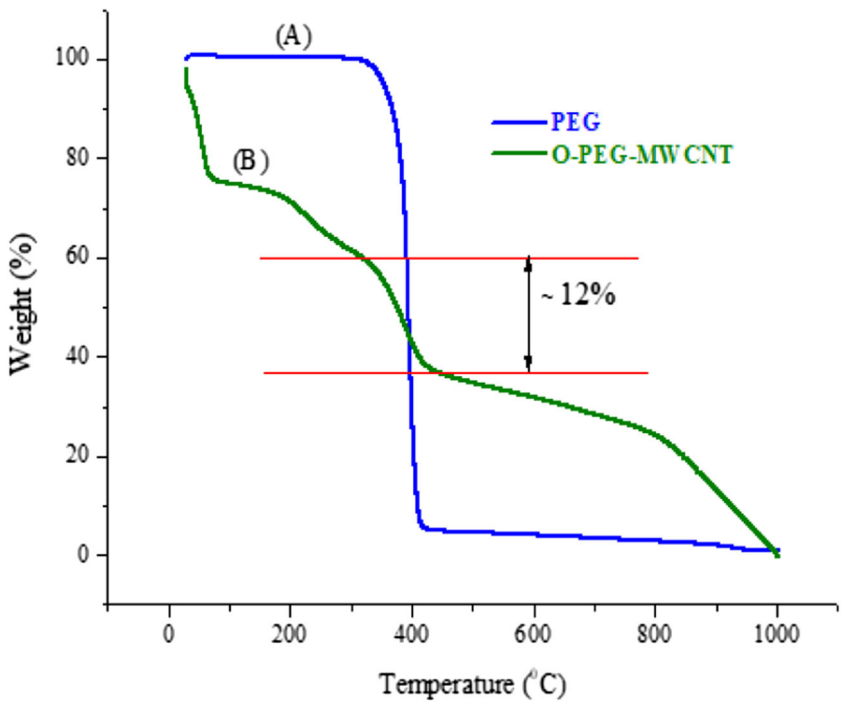

Fig. 4 TGA pattern for PEG and O-PEG-MWCNTs

TGA analysis: The thermal stability of nanocomposite and amount of PEG loaded onto O-MWCNTs were investigated based on TGA technique. Thermograms for neat PEG and functionalized O-PEG-MWCNTs are shown in Fig. 4(a) and (b) respectively. As can be seen (A), the neat PEG is lost 95% of weight at 300 °C. Figure 4(b) is showing four weight loss steps for O-PEG-MWCNTs, the first step at 100 °C is attributed residual moisture, second step at 200–300 °C is corresponding to the carboxyl groups of O-MWCNTs. Further weight loss was observed around 330–420 °C that demonstrates the decomposition of the loaded PEG. Hence, this is demonstrated that the 12% of O-PEG-MWCNTs is corresponding to grafted PEG chains. The forth mass loss which started around 800 °C belongs to decomposition of MWCNTs.

Adsorption kinetic

The impact of the incubation time on CUR uptake onto O-PEG-CNT was studied in order to select the optimum time for the most efficient loading of CUR drug. Figure 5(a) shows the adsorption capacity (q_t) at time t versus time (h). It demonstrated a drastic first jump from 800 mg/g at 1 h to 1000 mg/g at 5 h. According to Fig. 5(a) it can be seen that the loading capacity equilibrium at time t could reach the maximum (1200 mg/g) in an incubation period of time of 10–25 h. Hence, longer equilibrium time may be explained by the CUR sludge like adsorption over the sorbent surface which could be visualized by TEM [23]. Besides, slow adsorption is due to CNTs aggregation that disfavors the fast diffusion into the pores and internal CNT tubes [41]. Although equilibrium time is long, a noticeable adsorption capacity (800 mg/g) was obtained after 1 h. This may be explained by the enhanced surface area and dispersity of the PEGylated O-MWCNT tackling the high efficient drug delivery [42]. Fast adsorption of 800 mg CUR onto the sorbent within 1 h may be attributed to the interactions occurring at the surface of the O-PEG-CNTs material [41].

The experimental adsorption data were validated by the well-known pseudo-first-order and pseudo-second-order kinetic models (Eqs. 4 and 5 respectively) are listed in Table 1

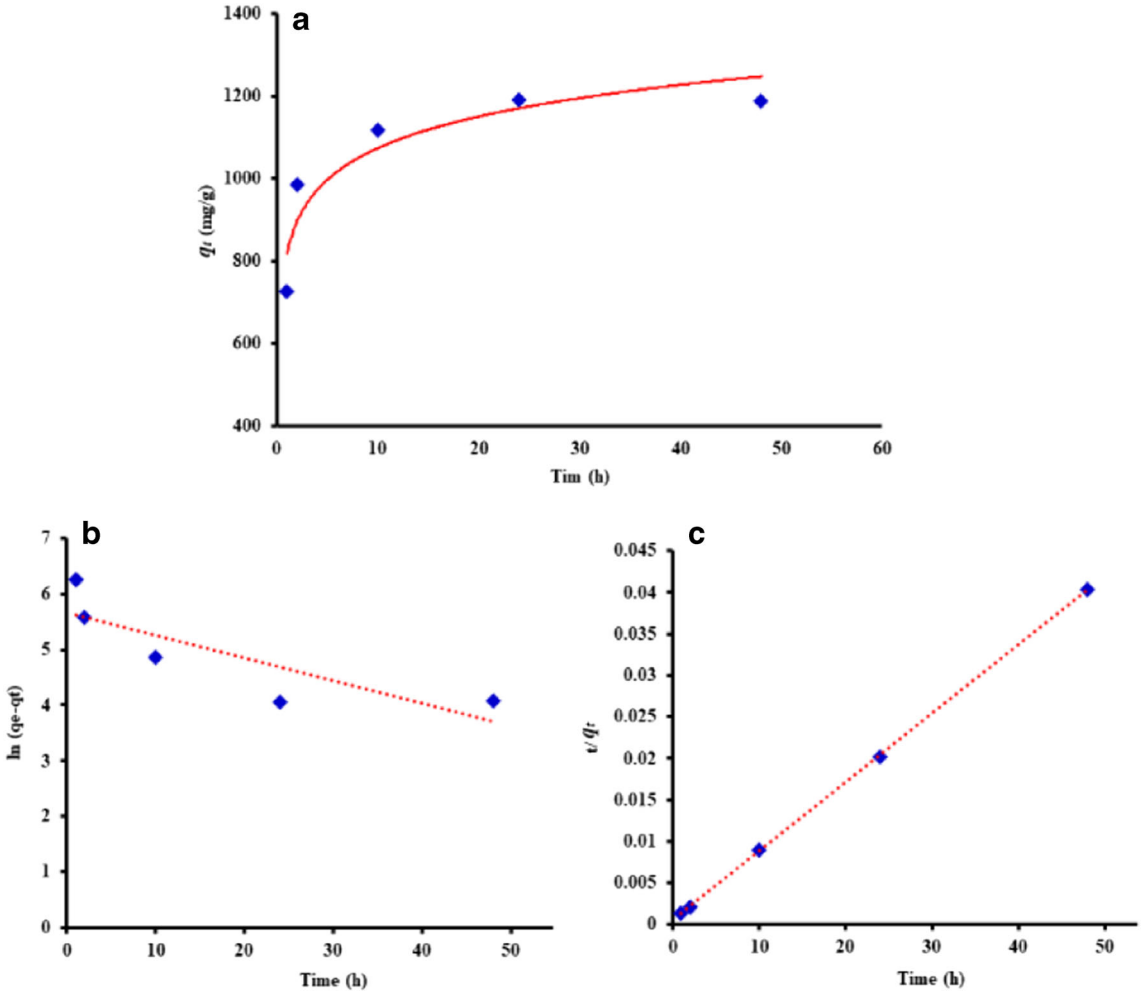

Fig. 5 (**a**) Effect of the contact time on adsorption capacity at time t. Kinetic analysis of CUR adsorption onto O-PEG-MWCNT by (**b**) pseudo-first-order and (**c**) pseudo-second-order models

Table 1 Kinetic study models, parameters and correlation coefficients for adsorption of CUR onto O-PEG-MWCNT

Model	Equation	Parameters	CUR
Pseudo-first-order	$ln(q_e - q_t) = ln\ q_e - k_1 t$ (4)	q_e (mg/g)	541.2
		k_1 (1/min)	0.084
		R^2	0.898
Pseudo-second-order	$\frac{t}{q_t} = \frac{1}{k_2 q_e^2} + \frac{1}{q_e}$ (5)	q_e (mg/g)	76.92
		k_2 (g/mg.min)	0.0012
		R^2	0.999

[43, 44]. The parameters can be explain as k_1 (min^{-1}) and k_2 (g/mg min) are the pseudo first and pseudo second order constants respectively, while q_t and q_e represent the amount of CUR adsorbed onto O-PEG-CNT at any time t (min) and the experimental sorption capacity at equilibrium (at 25 h) respectively (mg/g). The parameters q_e (theoretical) and k values of each model were calculated from the slope and intercept of the linear plots respectively (Fig. 5 b & c). The parameters' values stated in Table 1 that the pseudo-second-order model has resulted in a better fit displaying higher determination coefficient R^2 (0.999 > 0.898). Hence, this could be chosen as the ideal kinetic model for describing the adsorption of CUR onto O-PEG-MWCNTs.

Adsorption isotherm

The effect CUR initial concentration the on sorption equilibrium capacity of O-PEG-MWCNT (10 mg) was studied. Herein the initial concentration of CUR was varied from 50 to 1000 mg/L while the incubation time of 5 h was kept constant and the q_e vs C_e was recorded. As shown in Fig. 6 (a), the expected q_e increases by the increase of the initial concentration until CUR adsorption onto O-PEG-CNT reaches saturation at 1800 mg/g. The further increase in the concentration leads to a negligible increase in q_e which reaches a plateau value of 1800–2000 mg/g showing the agreeable performance of O-PEG-MWCNT for the CUR uptake.

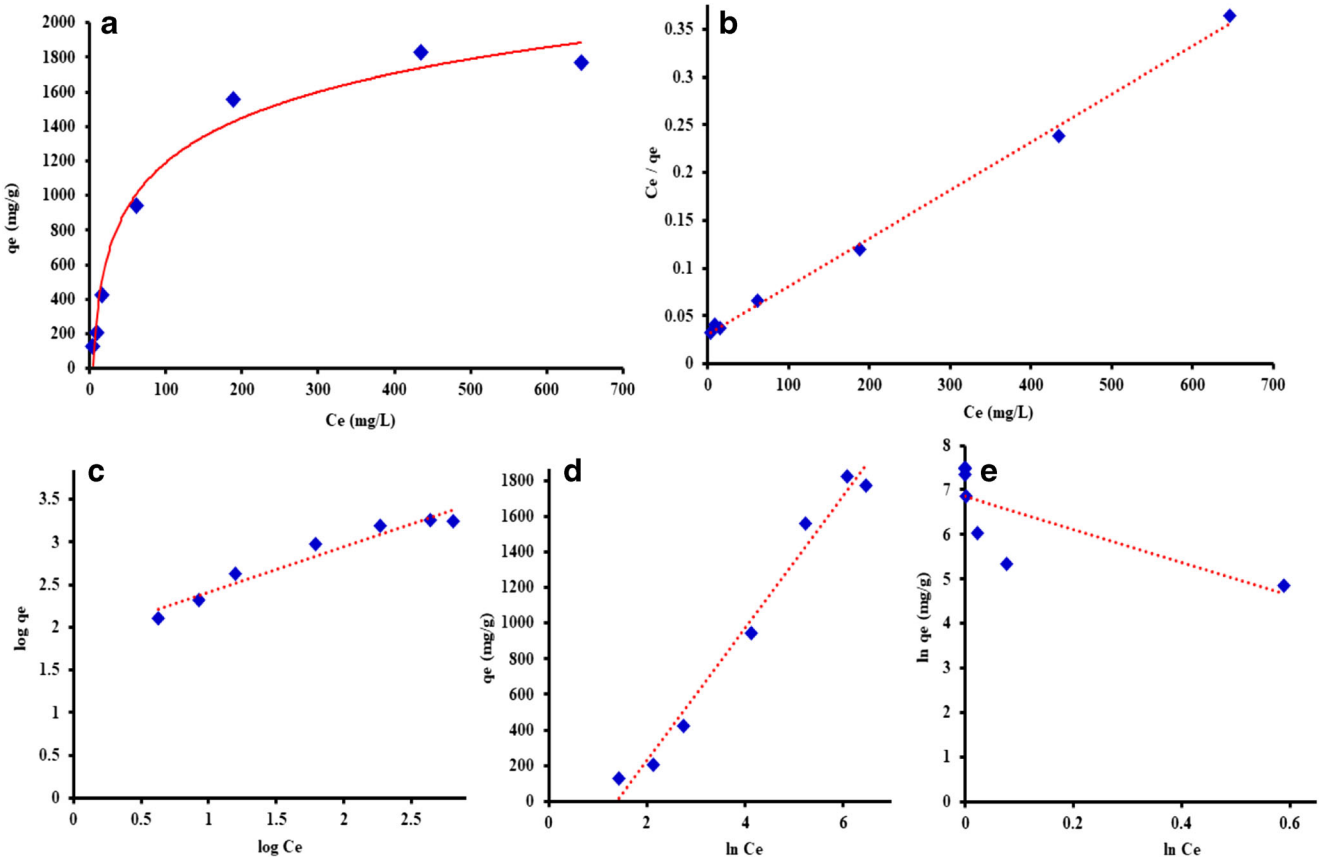

Fig. 6 (**a**) Adsorption isotherm equilibrium at different initial concentrations of CUR. Linear plot of the (**b**) Langmuir, (**c**) Freundlich, (**d**) Temkin and (**e**) Dubinin-Radushkevich isotherm models

Adsorption equilibrium process of CUR onto O-PEG-MWCNT was validated with isotherm models namely Langmuir, Freundlich, Temkin and Dubinin-Radushkevich. The models objectives are to predict the adsorption mechanism and to estimate the maximum adsorption capacity of the adsorbent. Langmuir isotherm states a monolayer formation of adsorbate on the adsorbent surface with no further adsorption and formation of additional layers assuming no transmigration and uniform adsorption energies, while Freundlich describes heterogeneous surfaces and a multilayer physisorption based adsorption [43, 45]. Temkin takes into account the indirect adsorbate-adsorbent interactions and the heat of adsorption on the adsorbent surface [46, 47]. Dubinin-Radushkevich describe a multilayer adsorption pattern with van der Waals forces [48, 49]. The linear Eqs. (6, 7, 8 and 9) for the proposed models and their parameters are expressed in Table 2 [43, 50]. Equation parameters are as C_e the residual concentration of CUR in solution (mg/L), q_e amount of CUR adsorbed onto O-PEG-MWCNT after reaching equilibrium (mg/g), q_m the maximum monolayer adsorption capacity (mg/g) of the adsorbent and K_L the Langmuir constant (L/mg) which is calculated from the slope and intercept of the linear plot (Fig. 6b), respectively. The intensity of adsorption (*n*) and Freundlich constant of K_F ((mg/g)/(mg/g)$^{1/n}$) could be obtained from the intercept and slope of linear graph, respectively (Fig. 6c). *B* is the Temkin constant related to the heat of sorption and *A* is the Temkin equilibrium binding constant (L/mg) corresponding to the maximum binding energy [51] calculated from slope and intercept of the linear plot, respectively (Fig. 6d). q_s (mg/g) and K_{ad} (mol^2 / kJ^2) are respectively the Dubinin's theoretical sorption capacity and constant equal to the intercept an slope of plot Fig. 6e [52]. *R* is the universal gas constant (8.314 J.mol/K), *T* is the temperature (K) and *E* corresponds to the adsorption free energy (kJ/mol) [51, 53]. The E values less than 8 kJ/mol correspond to a physical adsorption. The values between 8 to16 kJ/mol reflect an ion exchange mechanism [54] and ones higher than 20 kJ/mol describe a chemisorption mechanism [44, 55].

Figure 6a–d and Table. 2 show that the Langmuir-fitted plot provided a higher R^2 value (0.997 > 0.979 > 0.945 > 0.557) for the adsorption data compared to Temkin, Freundlich and Dubinin isotherm models. It could be notably stated that even after reaching an equilibrium time the mechanism of CUR adsorption onto O-PEG-MWCNTs continued in a monolayer pattern. The Langmuir's maximum adsorption capacity (q_m) of O-PEG-MWCNTs was obtained 2×10^3 mg/g showing the superiority of the PEGylated O-MWCNT sorbent as compared with pristine CNTs (769.23 mg/g) and oxygenated CNTs (714 mg/g) [56]. However, it was lower than that of PVA-MWCNT (3333 mg/g) [56]. The low Temkin constant of *A* (0.025 L/mg) and Langmuir's K_L (0.017 L/mg) values indicate a weak interaction between the CUR and the sorbent [51]. The high value of *1/n* in Freundlich isotherm denotes for an decrease in the CUR coverage onto the sorbent. Lastly, the low value of free energy ($E < 8$ kJ/mol) implies the physical adsorption mechanism of CUR uptake onto O-PEG-MWCNTs nanocomposite [54].

In vitro release of CUR from O-PEG-MWCNTs

The in vitro experiments were performed for studying the release behavior of the synthesized sorbent in different human fluids and organs (buffer ABS pH 5, intestinal fluid (SIF) pH 6.6 and body fluid (SBF) pH 7.4). It is noteworthy that CUR shows a very low solubility and desorption tendency at very low acidic pHs. As could be seen in Fig. 7a, all plots show the same initial increasing trend in the release of CUR during the first hour. At pH 7.4 this trend shows a steeper rate which leads to the highest plateau (~70%) and the most extended controlled release throughout the time scale. At pH 5

Table 2 Parameters and values of Langmuir, Freundlich, Temkin and Dubinin-Radushkevich models and free energy for the adsorption of CUR

Model	Equation	Isotherm constant	CUR
Langmuir	$\frac{C_e}{q_e} = \frac{C_e}{q_m} + \frac{1}{kq_m}$ (6)	q_m (mg/g)	2.0×10^3
		k (L/mg)	0.017
		R^2	0.997
Freundlich	$log\, q_e = log\ K_F + (1/n)\, log\ C_e$ (7)	K_F [(mg/g)/(mg/g)$^{1/n}$]	75.85
		1/n	1.88
		R^2	0.945
Temkin	$q_e = BlnA + BlnC_e$ (8)	A (L/mg)	0.025
		B (kJ/mol)	371
		R^2	0.979
Dubinin-Radushkevich	$ln\, q_e = ln\ q_s - K_{ad}(\varepsilon^2)$ (9) $\varepsilon = RT\ ln(1 + 1/C_e)$ (9.1)	q_s (mg/g)	910
		k_{ad} (mol^2/kJ)	−3.704
		R^2	0.557
Free energy	$E = 1/\sqrt{(-2K_{ad})}$ (10)	E (kJ/mol)	0.367

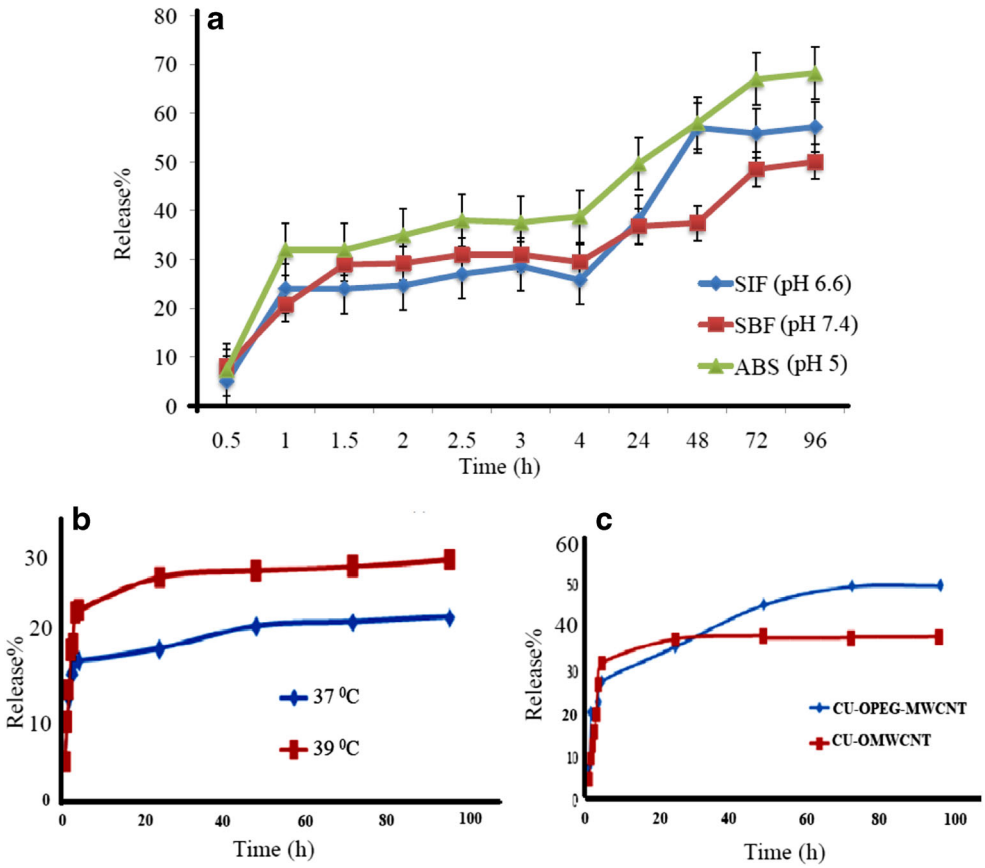

Fig. 7 (**a**) Release or desorption of CUR from O-PEG-MWCNT in simulated body fluids (buffer ABS pH 5, intestinal fluid (SIF) pH 6.6 and body fluid (SBF) pH 7.4) at 37 °C. (**b**) Effect of temperature on CUR desorption from O-PEG-MWCNT-CUR at pH 5. (**c**) Effect of polymer modification on CUR desorption from O-PEG-MWCNT-CUR

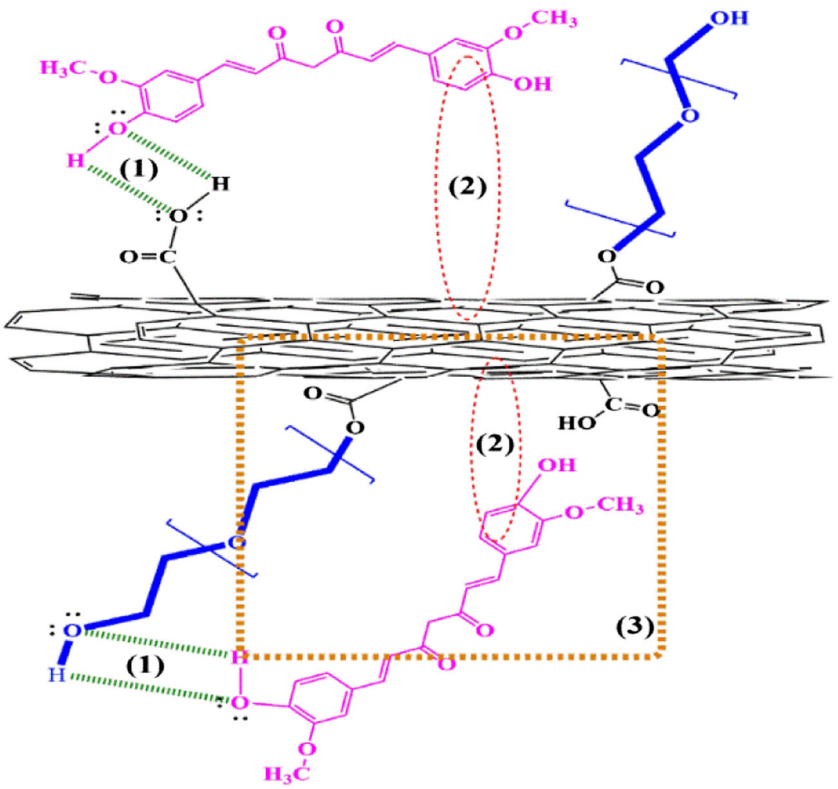

Fig. 8 Proposed sorption mechanism for adsorption of CUR by O-PEG-MWCNTs; hydrogen bonding (**1**), π-π interaction (**2**), and van der Waals forces (**3**)

(ABS), the release is only limited to 32% of adsorbed CUR, followed by a sustainable release of CUR for a period of 96 h (4 days) with percentage capacities from 32% to 68.2% for the desorption of CUR from O-PEG-MWCNTs. The higher release at slightly lower pHs (ABS 5) might be related to the increased stability of curcumin in acidic pH conditions due to the diene conjugation in its chemical structure [23]. Besides, the electrostatic interactions ccould occur between CUR and the protonation/deprotonation transitions of the O-PEG-CNTs material [57]. At pH 6.6 (SIF), the release rate obtained were 24.03% and 57.2% respectively after 1 and 96 h. At pH 7.4, the desorption of CUR is about 20.7% after 1 h, which is much lower than its desorption at pH 5 and pH 6.6. It has been reported that the pH of solid tumor (pH 5) is lower than that of a normal tissue (pH 7.4). Thus, the better release of CUR in pH 5 obtained in this work could help a successful release of CUR drug in tumor vicinity.

Effect of temperature on CUR release

The release behavior of O-PEG-MWCNTs for CUR at pH 5 was studied at two different temperatures (37and 39 °C) (Fig. 7b). It could be noted that there is a significant difference in the release rate of CUR at 37 °C and 39 °C with desorption efficiency percentages of 23 and 30.3% respectively. The release rates of CUR within the first hour at 37 °C and 39 °C were 0.233 mg/h and 0.281 mg/h respectively confirming a faster and more favorable release for CUR at 39 °C compared to 37 °C. The increase in temperature leads to an increase in the diffusion rate of CUR thus attributing to a higher release rate of the drug [58].

Effect of polymer on release rate of CUR

Note that the slow release rate that extended over several days prevents the unfavorable abrupt burst effect and enables the circulatory action of the drug [59]. The PEG modified MWCNT exhibited (Fig. 7c) an improves sustainability with the additional delay to the release of CUR compared to the MWCNTs. As could be seen, after 100 h, the O-PEG-MWCNTs showed >50% release in buffer (pH 5), while O-MWCNTs showed 37%. This result indicated a longer and more efficient release for O-PEG-MWCNTs compared to O-MWCNTs which approved the success of the designed adsorbent. According to the literature, covalently grafted PEG brushes show an agreeable dispersability and a long circulation time. Therefore, these properties make PEG functionalized CNT a favorable platform for CUR delivery.

Adsorption mechanism

Figure 8 represents the proposed adsorption mechanism of CUR uptake onto O-PEG-MWCNTs. A great portion of adsorption may be traced the surface OH groups of CNTs and PEG (as the donor) can interact with carbonyl groups (COOH) of CUR as the acceptor followed by hydrogen bonding) Fig. 8(1)([27, 57]. The large π-stacking of the aromatic rings of adsorbent and adsorbate may established the π-π interactions between the CUR and O-PEG-MWCNT Fig. 8(2) [58]. Finally, the hydrophobic nature of adsorbent and adsorbate involve the hydrophobic interactions via van der Waals forces (Fig. 8(**3**)).

Conclusion

In summary, the in vitro adsorption/release of CUR drug from O-PEG-MWCNTs was studied in different conditions in order to fine-tune the nanocomposite in a drug delivery system. The proper isotherm modelling and evaluations verified the physical loading of CUR onto the proposed adsorbent. The Langmuir adsorption model best-fitted with the experimental data and well-explained the adsorption process and predicted a high maximum sorption capacity of 2×10^3 mg/g for CUR with a monolayer coverage on the surface of synthesized nanocomposite. This high adsorption capacity might be related to the dominant favorable there interaction as π-π interactions, van der Waals forces and hydrogen bonding between CUR and O-PEG-MWCNTs. A very efficient and prolonged drug release ability was observed using O-PEG-MWCNTs in three simulated fluids: ABS pH 5, SIF pH 6.6 and SBF pH 7.4. This led to a controlled efficient drug delivery system for a desired sustained release of the drug rather than the unfavorable abrupt burst release of CUR. This is likely to reduce toxicity and other drug related side effects in the clinical studies that thought to be necessary to improve the therapy.

Acknowledgments Authors would like to thanks Universiti Teknologi Malaysia (UTM) for the facilities and financial support.

Compliance with ethical standards

Conflict of interest "Authors declare that there is no conflict of interest".

Publisher's Note Springer Nature remains neutral with regard to jurisdictional claims in published maps and institutional affiliations.

References

1. Rathaur P, Raja W, Ramteke PW, John SA. Turmeric: the golden spice of life. Int J Pharm Sci Res. 2012;3:1987.
2. Hussain Z, Thu HE, Amjad MW, Hussain F, Ahmed TA, Khan S. Exploring recent developments to improve antioxidant, anti-inflammatory and antimicrobial efficacy of curcumin: a review of

new trends and future perspectives. Mater Sci Eng C. 2017;77: 1316–26.
3. Attari F, Zahmatkesh M, Aligholi H, Mehr SE, Sharifzadeh M, Gorji A. Curcumin as a double-edged sword for stem cells: dose, time and cell type-specific responses to curcumin. DARU J Pharm Sci. 2015;23:33.
4. Naksuriya O, Okonogi S, Schiffelers RM, Hennink WE. Curcumin nanoformulations: a review of pharmaceutical properties and preclinical studies and clinical data related to cancer treatment. Biomaterials. 2014;35:3365–83.
5. Chougala MB, Bhaskar JJ, Rajan MGR, Salimath PV. Effect of curcumin and quercetin on lysosomal enzyme activities in streptozotocin-induced diabetic rats. Clin Nutr. 2012;31:749–55.
6. Anand P, Kunnumakkara AB, Newman RA, Aggarwal BB. Bioavailability of curcumin: problems and promises. Mol Pharm. 2007;4:807–18.
7. Chattopadhyay I, Biswas K, Bandyopadhyay U, Banerjee RK. Turmeric and curcumin: biological actions and medicinal applications. Curr Sci. 2004;87:44–53.
8. Cha T-G, Pan J, Chen H, Salgado J, Li X, Mao C, et al. A synthetic DNA motor that transports nanoparticles along carbon nanotubes. Nat Nanotechnol. 2014;9:39–43.
9. Jafari A, Ghorannevis Z, Ghoranneviss M, Karimi S. Nitrogen ion bombardment of multilayer graphene films grown on cu foil by LPCVD. Int J Mater Res. 2016;107:177–83.
10. Liu Z, Tabakman S, Welsher K, Dai H. Carbon nanotubes in biology and medicine: in vitro and in vivo detection, imaging and drug delivery. Nano Res. 2009;2:85–120.
11. Ji S, Liu C, Zhang B, Yang F, Xu J, Long J, et al. Carbon nanotubes in cancer diagnosis and therapy. Biochim Biophys Acta - Rev Cancer. 2010;1806:29–35.
12. Hadavifar M, Bahramifar N, Younesi H, Li Q. Adsorption of mercury ions from synthetic and real wastewater aqueous solution by functionalized multi-walled carbon nanotube with both amino and thiolated groups. Chem Eng J. 2014;237:217–28.
13. Liu X, Tao H, Yang K, Zhang S, Lee S-T, Liu Z. Optimization of surface chemistry on single-walled carbon nanotubes for in vivo photothermal ablation of tumors. Biomaterials. 2011;32:144–51.
14. Klingeler R, Hampel S, Büchner B. Carbon nanotube based biomedical agents for heating, temperature sensoring and drug delivery. Int J Hyperth Taylor & Francis. 2008;24:496–505.
15. Mahajan S, Patharkar A, Kuche K, Maheshwari R, Deb PK, Kalia K, et al. Functionalized carbon nanotubes as emerging delivery system for the treatment of cancer. Int J Pharm. 2018;548:540–58.
16. Shuit SH, Ng EP, Tan SH. A facile and acid-free approach towards the preparation of sulphonated multi-walled carbon nanotubes as a strong protonic acid catalyst for biodiesel production. J Taiwan Inst Chem Eng E. 2015;52:100–8.
17. Madani SY, Naderi N, Dissanayake O, Tan A. Seifalian AM. A new era of cancer treatment: carbon nanotubes as drug delivery tools. Int J Nanomedicine. 2011;6:2963–79.
18. Liu Z, Fan AC, Rakhra K, Sherlock S, Goodwin A, Chen X. Supramolecular stacking of doxorubicin on carbon nanotubes for in vivo Cancer therapy. Angew Chemie Int Ed. 2009;48:7668–72.
19. Lu Y-J, Wei K-C, Ma C-CM, Yang S-Y, Chen J-P. Dual targeted delivery of doxorubicin to cancer cells using folate-conjugated magnetic multi-walled carbon nanotubes. Colloids Surfaces B Biointerfaces. 2012;89:1–9.
20. Meena S, Choudhary S. Effects of functionalization of carbon nanotubes on its spin transport properties. Mater Chem Phys. 2018;217: 175–81.
21. Wang Z, Zhao J, Song L, Mashayekhi H, Chefetz B, Xing B. Adsorption and desorption of Phenanthrene on carbon nanotubes in simulated gastrointestinal fluids. Environ Sci Technol. 2011;45: 6018–24.
22. Yan XM, Shi BY, Lu JJ, Feng CH, Wang DS, Tang HX. Adsorption and desorption of atrazine on carbon nanotubes. J Colloid Interface Sci. 2008;321:30–8.
23. Wang Y, Yang S-T, Wang Y, Liu Y, Wang H. Adsorption and desorption of doxorubicin on oxidized carbon nanotubes. Colloids Surfaces B Biointerfaces. 2012;97:62–9.
24. Oleszczuk P, Pan B, Xing B. Adsorption and desorption of Oxytetracycline and carbamazepine by multiwalled carbon nanotubes. Environ Sci Technol. 2009;43:9167–73.
25. Zeinabad HA, Zarrabian A, Saboury AA, Alizadeh AM, Falahati M. Interaction of single and multi wall carbon nanotubes with the biological systems: tau protein and PC12 cells as targets. Sci Rep. 2016;6:26508.
26. Tofighy MA, Mohammadi T. Adsorption of divalent heavy metal ions from water using carbon nanotube sheets. J Hazard Mater. 2011;185:140–7.
27. Vasconcelos T, Sarmento B, Costa P. Solid dispersions as strategy to improve oral bioavailability of poor water soluble drugs. Drug Discov Today. 2007;12:1068–75.
28. D'souza AA, Shegokar R. Polyethylene glycol (PEG): a versatile polymer for pharmaceutical applications. Expert Opin Drug Deliv. 2016;13:1257–75.
29. Bhattacharya K, Sacchetti C, Costa PM, Sommertune J, Brandner BD, Magrini A. Nitric oxide dependent degradation of polyethylene glycol-modified single-walled carbon nanotubes: implications for intra-articular delivery. Adv Healthc Mater. 2018;7:1700916.
30. Dolatimehr F, Karimi-Sari H, Rezaee-Zavareh MS, Alavian SM, Behnava B, Gholami-Fesharaki M, et al. Combination of sofosbuvir, pegylated-interferon and ribavirin for treatment of hepatitis C virus genotype 1 infection: a systematic review and meta-analysis. DARU J Pharm Sci. 2017;25:11.
31. Novaes LC de L, Jozala AF, Mazzola PG, Júnior AP, Novaes LC de L, Jozala AF, et al. The influence of pH, polyethylene glycol and polyacrylic acid on the stability of stem bromelain. Brazilian J Pharm Sci. 2014;50:371–80.
32. Davarpanah F, Yazdi AK, Barani M, Mirzaei M, Torkzadeh-Mahani M. Magnetic delivery of antitumor carboplatin by using PEGylated-Niosomes. DARU J Pharm Sci. 2018;26:57–64.
33. Sarier N, Onder E. Organic modification of montmorillonite with low molecular weight polyethylene glycols and its use in polyurethane nanocomposite foams. Thermochim Acta. 2010;510:113–21.
34. AM K, Rashid NA. Study of stability and Dispersibility of oxidized multiwall carbon nanotube and characterization with analytical methods for bioapplication. J Chem Health Ris. 2011;1:17–22.
35. Balaji RA, Raghunathan S, Revathy R. Levofloxacin: formulation and in-vitro evaluation of alginate and chitosan nanospheres. Egypt Pharm J. 2015;14:30–5.
36. Shi X, Zheng Y, Wang G, Lin Q, Fan J. pH-and electro-response characteristics of bacterial cellulose nanofiber/sodium alginate hybrid hydrogels for dual controlled drug delivery. RSC Adv. 2014;4: 47056–65.
37. Zhou Y, Pervin F, Lewis L, Jeelani S. Fabrication and characterization of carbon/epoxy composites mixed with multi-walled carbon nanotubes. Mater Sci Eng A. 2008;475:157–65.
38. Su F, Lu C, Hu S. Adsorption of benzene, toluene, ethylbenzene and p-xylene by NaOCl-oxidized carbon nanotubes. Colloids Surfaces A Physicochem Eng Asp. 2010;353:83–91.
39. Branca C, Frusteri F, Magazù V, Mangione A. Characterization of carbon nanotubes by TEM and infrared spectroscopy. J Phys Chem B. 2004;108:3469–73.
40. Sreeprasad TS, Maliyekkal SM, Lisha KP, Pradeep T. Reduced graphene oxide-metal/metal oxide composites: facile synthesis and application in water purification. J Hazard Mater. 2011;186: 921–31.

41. Viseras MT, Aguzzi C, Cerezo P, Viseras C, Valenzuela C. Equilibrium and kinetics of 5-aminosalicylic acid adsorption by halloysite. Microporous Mesoporous Mater. 2008;108:112–6.
42. Zhang W, Zhang Z, Zhang Y. The application of carbon nanotubes in target drug delivery systems for cancer therapies. Nanoscale Res Lett. 2011;6:555.
43. Mohammadi Nodeh MK, Gabris MA, Rashidi Nodeh H, Esmaeili Bidhendi M. Efficient removal of arsenic(III) from aqueous media using magnetic polyaniline-doped strontium–titanium nanocomposite. Environ Sci Pollut Res. 2018;25:16864–74.
44. Rashidi Nodeh H, Sereshti H. Synthesis of magnetic graphene oxide doped with strontium titanium trioxide nanoparticles as a nanocomposite for the removal of antibiotics from aqueous media. RSC Adv. 2016;6:89953–65.
45. Dada A. Olalekan, Olatunya AM, Dada. Langmuir, Freundlich, Temkin and Dubinin–Radushkevich isotherms studies of equilibrium sorption of Zn^{2+} unto phosphoric acid modified Rice husk. IOSR J Appl Chem. 3:2278–5736.
46. Dehghani MH, Sanaei D, Ali I, Bhatnagar A. Removal of chromium (VI) from aqueous solution using treated waste newspaper as a low-cost adsorbent: kinetic modeling and isotherm studies. J Mol Liq. 2016;215:671–9.
47. Foo KY, Hameed BH. Insights into the modeling of adsorption isotherm systems. Chem Eng J. 2010;156:2–10.
48. Luo S, Xu X, Zhou G, Liu C, Tang Y, Liu Y. Amino siloxane oligomer-linked graphene oxide as an efficient adsorbent for removal of Pb(II) from wastewater. J Hazard Mater. 2014;274:145–55.
49. Boparai HK, Joseph M, O'Carroll DM. Kinetics and thermodynamics of cadmium ion removal by adsorption onto nano zerovalent iron particles. J Hazard Mater. 2011;186:458–65.
50. Nodeh HR, Sereshti H, Afsharian EZ, Nouri N. Enhanced removal of phosphate and nitrate ions from aqueous media using nanosized lanthanum hydrous doped on magnetic graphene nanocomposite. J Environ Manag. 2017;197:265–74.
51. Khan TA, Chaudhry SA, Ali I. Equilibrium uptake, isotherm and kinetic studies of cd (II) adsorption onto iron oxide activated red mud from aqueous solution. J Mol Liq. 2015;202:165–75.
52. Alizadeh Eslami P, Kamboh MA, Rashidi Nodeh H, Wan Ibrahim WA. Equilibrium and kinetic study of novel methyltrimethoxysilane magnetic titanium dioxide nanocomposite for methylene blue adsorption from aqueous media. Appl Organomet Chem. 2018;32:e4331.
53. Gabris MA, Jume BH, Rezaali M, Shahabuddin S, Rashidi Nodeh H, Saidur R. Novel magnetic graphene oxide functionalized cyanopropyl nanocomposite as an adsorbent for the removal of Pb (II) ions from aqueous media: equilibrium and kinetic studies. Environ Sci Pollut Res. 2018;25:27122–32.
54. Ngo HH, Guo W, Zhang J, Liang S, Ton-That C, Zhang X. Typical low cost biosorbents for adsorptive removal of specific organic pollutants from water. Bioresour Technol. 2015;182:353–63.
55. Wang W, Li M, Zeng Q. Thermodynamics of Cr (VI) adsorption on strong alkaline anion exchange fiber. Trans Nonferrous Met Soc China. 2012;22:2831–9.
56. Zawawi NA, Majid ZA, Rashid NAA. Adsorption and desorption of curcumin by poly (vinyl) alcohol-multiwalled carbon nanotubes (PVA-MWCNT). Colloid Polym Sci. 2017;295:1925–36.
57. Yang P, Quan Z, Li C, Kang X, Lian H, Lin J. Bioactive, luminescent and mesoporous europium-doped hydroxyapatite as a drug carrier. Biomaterials. 2008;29:4341–7.
58. Gao Y, Li Y, Zhang L, Huang H, Hu J, Shah SM. Adsorption and removal of tetracycline antibiotics from aqueous solution by graphene oxide. J Colloid Interface Sci. 2012;368:540–6.
59. Wang H, Chen J, Xu C, Shi L, Tayier M, Zhou J, et al. Cancer nanomedicines stabilized by π-π stacking between heterodimeric prodrugs enable exceptionally high drug loading capacity and safer delivery of drug combinations. Theranostics. 2017;7:3638–52.